



Inhomogeneous MUSIG Model – a Population Balance Approach for Polydispersed Bubbly Flows

Thomas Frank
ANSYS Germany GmbH
Staudenfeldweg 12, D-83624 Otterfing
Germany
Thomas.Frank@ansys.com

Philip J. Zwart
ANSYS Canada Ltd.
554 Parkside Drive, Waterloo
Ontario N2L 5Z4, Canada
Phil.Zwart@ansys.com

Jun-Mei Shi¹, Eckhart Krepper², Dirk Lucas, Ulrich Rohde
FZ Rossendorf – Institute of Safety Research
P.Box 510119, D-01314 Dresden
Germany

¹J.Shi@fz-rossendorf.de, ²E.Krepper@fz-rossendorf.de

ABSTRACT

Many flow regimes in Nuclear Reactor Safety (NRS) Research are characterized by multiphase flows, with one phase being a continuous liquid and the other phase consisting of gas or vapour of the liquid phase. In the range of low to intermediate volume fraction of the gaseous phase the multiphase flow under consideration is a bubbly or slug flow, where the disperse phase is characterized by an evolving bubble size distribution due to bubble breakup and coalescence processes. The paper presents a generalized inhomogeneous Multiple Size Group (MUSIG) Model. Within this model the disperse gaseous phase is divided into N inhomogeneous velocity groups (phases) and each of these groups is subdivided into M bubble size classes. Bubble breakup and coalescence processes between all bubble size classes are taken into account by appropriate models. The derived inhomogeneous MUSIG model has been validated against experimental data from the TOPFLOW test facility at the Research Center Rossendorf (FZR). Comparisons of gas volume fraction and velocity profiles with TOPFLOW-074 test case data are provided, showing the applicability and accuracy of the model for polydispersed bubbly flow in large diameter vertical pipe flow.

1 INTRODUCTION

Considering gas-liquid flows in vertical pipes, the flow morphology largely depends on the volume fraction of the gaseous phase. If the void fraction of the gaseous phase is increased, the flow regime changes from bubbly flow to slug flow, churn turbulent flow, annular flow, and finally to droplet flow. Flow morphology changes in gas-liquid flows had been studied experimentally for many years by establishing so-called flow maps. There is so far no general multiphase flow model which is capable of accurately predicting gas-liquid flows in all these flow regimes or even transition between different flow regimes. If we reduce the scope to the

range of gaseous phase volume fraction where we observe bubbly or slug flow, then the multiphase flow is characterized by the following factors:

- The gas-liquid flow is determined by a spectrum of bubble sizes, which depends on the dispersed phase volume fraction and the method of gas injection for the bubbly/slug flow. Flows with low gas volume fraction are mostly monodisperse, while increasing the gas volume fraction leads to a broader bubble size distribution due to bubble breakup and coalescence.
- Bubbles of different sizes are subject to lateral migration due to forces acting in the lateral directions. Due to the sign change in bubble lift force in accordance to the Tomiyama lift force coefficient correlation [1] this lateral migration leads to a demixing of small and large bubbles and to further coalescence of large bubbles migrating towards the pipe center into even larger Taylor bubbles or slugs.

Different attempts in MPF model development had been made in the past, in order to take bubble size distributions and bubble breakup and coalescence processes into account. Sommerfeld et al. [2], [3] developed a Lagrangian bubble tracking approach. The representation of a particle/bubble size distribution in a Lagrangian simulation is straight forward by assigning different bubble diameters to different calculated trajectories. The bubble coalescence can be predicted from binary bubble collision processes using a stochastic inter-particle collision model. In this model bubble coalescence occurred in case that the contact time became larger than the film drainage time. The model has been applied and compared to measurements in bubble driven loop reactor flow showing reasonably good agreement. But so far Lagrangian bubble tracking methods are known to have their limitations for comparable small gas volume fractions.

Another approach is the DNS-like resolution of the interface and fluid flow around each individual bubble, like it is realized in VOF or front tracking methods. Large bubble systems of monodisperse and differently sized bubbles have been investigated by e.g. Bunner & Tryggvason [4], [5], Tomiyama [1], Götz et al. [6] and Wörner et al. [7], but mostly in simplified geometries under additional symmetry assumptions. The numerical effort of these methods is tremendous and therefore the applicability of the VOF and front tracking methods is currently limited to fundamental research and e.g. turbulence model development. Also the interaction of bubbles has been studied with these methods, difficulties in treatment of bubble breakup and coalescence are encountered by both VOF and front tracking algorithms.

The present paper focuses on the Eulerian framework of multiphase flow simulation. Here the MUSIG model by Lo [8] has led to some success in the prediction of industrial bubbly flows by taking the bubble size distribution into account. This model solves continuity and momentum equations for the continuous phase (liquid) and one single disperse phase (gas). In order to describe the size distribution of bubbles, continuity equations for different size groups are introduced and the coalescence and break-up processes are considered based on population balance method. Bubble break-up and coalescence are modeled in accordance with the models proposed by Luo & Svendsen [9] and Prince & Blanch [10]. The performance of this original MUSIG model – also referred to as the homogeneous MUSIG model due to the restriction to one gaseous phase velocity field – is limited to convectively dominated bubbly flows as e.g. in stirred vessel reactors, since it is based on the assumption of a homogeneous velocity field applied to all bubble size classes. The homogeneous MUSIG model is therefore not able to predict the lateral demixing of bubbles of different sizes under the flow regimes as described above.

Significant progress in the simulation of polydisperse gas-liquid flow could be established by applying a fully inhomogeneous multiphase flow simulation to the gas-liquid bubbly flows of higher gas concentration, where a coupled system of continuity and momentum equations is solved for the continuous liquid phase and a number N of disperse

bubbly phases. First a so-called NP2- or (N+1)-fluid model has been proposed by Tomiyama et al. [1], [11] and has been applied for N=3 to bubble plume simulations in a cylindrical bubble column. Appropriate source and sink terms account for the transfer in mass and momentum due to bubble breakup and coalescence between the different gaseous phases. Numerical simulations using CFX-10 with N=4 up to N=8 disperse phases have been carried out by Shi, Frank et al. [12], [13], [14] for different flow conditions in vertically upward bubbly pipe flows and were compared to measurements at the MT-Loop [15] and TOPFLOW [16] test facilities at FZR. Good agreement to experimental data could be established for the axial development of gas volume fraction profiles at different pipe elevations for bubbly flows with a broader bubble size distribution developing from small to large bubbles over the height of the vertical pipe.

These approaches may be described as fully inhomogeneous models, wherein each size group is permitted to move with its own velocity. However, for good accuracy, a large number of size groups (at least ~15-20) may be required for good resolution of the size distribution, and this method is very expensive in this situation. This observation provides motivation for the development of a more efficient multifluid-based population balance strategy, which we refer to as the inhomogeneous MUSIG model.

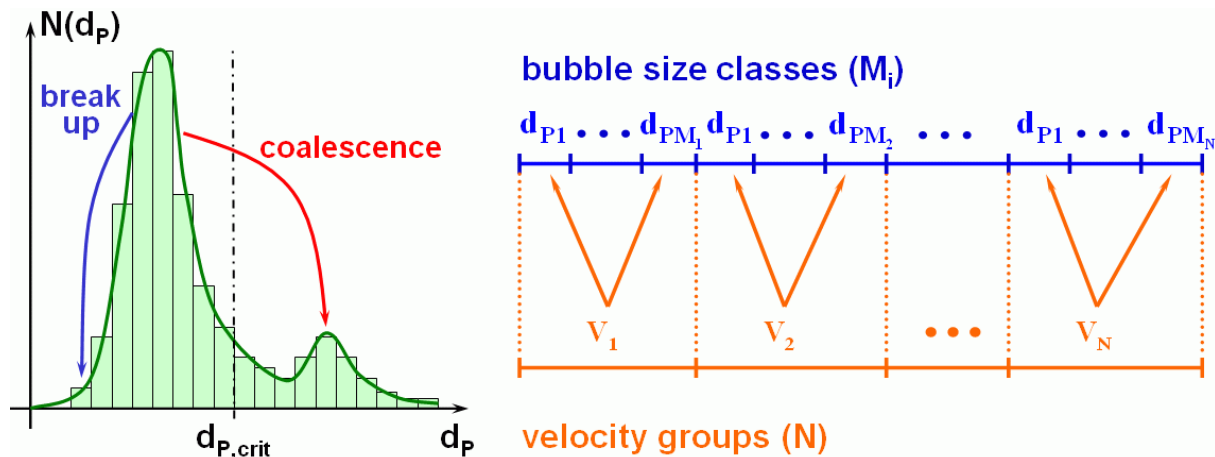


Figure 1: Velocity group and bubble size class subdivision of the bubble size spectrum in the inhomogeneous MUSIG model for polydisperse bubbly flow.

2 THE INHOMOGENEOUS MUSIG MODEL

2.1 Velocity Groups and Bubble Size Classes

A basic requirement for a multi-fluid model for polydisperse bubbly flows is to capture the radial demixing of small and large bubbles compared to the ‘critical’ bubble diameter in correspondence to the Tomiyama lift force coefficient correlation, where the lift force acting on a bubble is changing its direction. Therefore in the proposed inhomogeneous Multiple Size Group (MUSIG) model the gaseous disperse phase is divided into a number N so-called velocity groups (or phases), where each of the velocity groups is characterized by its own velocity field. The subdivision should be based on the physics of bubble motion for bubbles of different size, e.g. different behaviour of differently sized bubbles with respect to lift force or turbulent dispersion. Therefore it can be suggested, that in most cases 3 or 4 velocity groups should be sufficient in order to capture the main phenomena in bubbly or slug flows.

Further the overall bubble size distribution is represented by dividing the bubble diameter range within each of the velocity groups in a number M_i bubble size classes (see Fig. 1). The lower and upper boundaries of bubble diameter intervals for the bubble size classes can be controlled by either an equal bubble diameter distribution, an equal bubble mass distribution or can be based on user definition of the bubble diameter ranges for each distinct bubble diameter class. For simplicity it is further assumed, that the number of bubble diameter classes within each of the velocity groups is equal, i.e. $M=M_1=M_2= \dots = M_N$, also this is not a limitation of the model.

2.2 Model Formulation

The simulation of the gas-liquid polydispersed bubbly flow is based on the CFX-10 multi-fluid Euler-Euler approach [17]. The Eulerian modeling framework is based on ensemble-averaged mass and momentum transport equations for all phases/velocity groups. Regarding the liquid phase as continuum ($\alpha=1$) and the gaseous phase velocity groups (bubbles) as disperse phase ($\alpha=2, \dots, N+1$) these equations read:

$$\frac{\partial}{\partial t}(r_\alpha \rho_\alpha) + \nabla \cdot (r_\alpha \rho_\alpha \vec{U}_\alpha) = S_\alpha \quad (1)$$

$$\frac{\partial}{\partial t}(r_\alpha \rho_\alpha \vec{U}_\alpha) + \nabla \cdot (r_\alpha \rho_\alpha \vec{U}_\alpha \otimes \vec{U}_\alpha) = \quad (2)$$

$$\nabla \cdot (r_\alpha \mu_\alpha (\nabla \vec{U}_\alpha + (\nabla \vec{U}_\alpha)^T)) - r_\alpha \nabla p + r_\alpha \rho_\alpha \vec{g} + \vec{M}_\alpha + \vec{S}_{M\alpha}$$

$$\vec{M}_\alpha = \vec{F}_D + \vec{F}_L + \vec{F}_{WL} + \vec{F}_{TD} \quad (3)$$

where r_α , ρ_α , μ_α are the void fraction, density and viscosity of the phase α and \vec{M}_α represents the sum of interfacial forces like the drag force \vec{F}_D , lift force \vec{F}_L , wall lubrication force \vec{F}_{WL} and turbulent dispersion force \vec{F}_{TD} . The source terms S_α and $\vec{S}_{M\alpha}$ represent the transfer of gaseous phase mass and momentum between different velocity groups due to bubble breakup and coalescence processes leading to bubbles of certain size belonging to a different velocity group. Consequently these terms are zero for the liquid phase transport equations. Turbulence of the liquid phase has been modeled using Menter's $k-\omega$ based Shear Stress Transport (SST) model [17]. The turbulence of the disperse bubbly phase was modeled using a zero equation turbulence model and bubble induced turbulence has been taken into account according to Sato's model [17].

The interfacial drag and non drag force terms M_β with:

$$\vec{F}_D = \frac{3}{4} C_D \frac{r_\beta \rho_\alpha}{d_\beta} |\vec{U}_\alpha - \vec{U}_\beta| (\vec{U}_\alpha - \vec{U}_\beta) \quad (4)$$

$$\vec{F}_L = C_L r_\beta \rho_\alpha (\vec{U}_\alpha - \vec{U}_\beta) \times \nabla \times \vec{U}_\alpha \quad (5)$$

$$\vec{F}_{WL} = -C_{WL} r_\beta \rho_\alpha |\vec{U}_{rel} - (\vec{U}_{rel} \cdot \vec{n}_w) \vec{n}_w|^2 \vec{n}_w \quad (6)$$

$$\vec{F}_{TD} = D_{\alpha\beta} A_{\alpha\beta} \frac{v_{t\alpha}}{\sigma_{r\alpha}} \left(\frac{\nabla r_\alpha}{r_\alpha} - \frac{\nabla r_\beta}{r_\beta} \right) \quad (7)$$

where α denotes the liquid phase and β the properties of the corresponding gaseous phase velocity group, need further closure relations for the various force coefficients C_D , C_L , C_{WL} and model parameters like $\sigma_{r\alpha}$. In the present study the Grace [17] and Tomiyama drag coefficient [18], lift force coefficient [1] and wall lubrication force formulation of Tomiyama [1] and the so-called Favre averaged drag (FAD) turbulent dispersion model [19] were used.

The Tomiyama drag force coefficient correlation considers bubble drag in the distorted bubble regime similar to the Grace drag model built into CFX-10, but additionally contains a parameter considering the contamination of the air-water system. This contamination parameter has been set to $A=24$. The high gas void fraction correction exponent in the Tomiyama drag correlation was set to $n=4$. The given non-drag forces were implemented in CFX-10 and are available since the release of CFX-5.7 [19]. Other drag and non-drag force models can be implemented as well using user defined CFX command language (CCL) expressions or FORTRAN routines for the prediction of the various force coefficients.

2.3 Bubble Breakup and Coalescence

In the inhomogeneous MUSIG model the polydispersed gaseous phase is divided among a fixed number of $\sum_{i=1}^N M_i$ (or with our simplifying assumption $N \times M$) size groups, each representing a range of bubble sizes and where breakup and coalescence between all size groups is taken into account. Introducing r_d as the volume fraction of the cumulative disperse phase and $r_i = r_d \cdot f_i = r_{\alpha} \cdot f_{\alpha,i}$ the gas volume fraction in a single size group, then the continuity equations for the velocity group α , $\alpha \in [1, N]$ and the bubble size group i , $i \in [1, N \times M]$ read:

$$\frac{\partial}{\partial t}(\rho_d r_{\alpha}) + \frac{\partial}{\partial x^j}(\rho_d r_{\alpha} U_{\alpha}^j) = S_{\alpha} \quad (8)$$

$$\frac{\partial}{\partial t}(\rho_d r_{\alpha} f_{\alpha,i}) + \frac{\partial}{\partial x^j}(\rho_d r_{\alpha} f_{\alpha,i} U_{\alpha}^j) = S_{\alpha,i} \quad (9)$$

with the additional relations and constraints:

$$r_d = \sum_{\alpha=1}^N r_{\alpha} = \sum_{i=1}^{N \times M} r_i \quad , \quad r_{\alpha} = \sum_{i=1}^{M_{\alpha}} r_i \Big|_{vel.group \alpha} \quad (10)$$

$$r_i + r_d = 1 \quad , \quad \sum_{i=1}^{N \times M} f_i = 1 \quad , \quad \sum_{i=1}^{M_{\alpha}} f_{\alpha,i} \Big|_{vel.group \alpha} = 1$$

Here in eq. (9) the term $S_{\alpha,i}$ is the net rate at which mass accumulates in group i due to coalescence and breakup. Applying the breakup model of Luo & Svendsen [9] and the coalescence model of Prince & Blanch [10], this term can be written as:

$$\begin{aligned} S_{\alpha,i} &= B_{i,B} - D_{i,B} + B_{i,C} - D_{i,C} \\ &= \rho_d r_d \sum_{j>i} B_{ij} f_j - \rho_d r_d f_i \sum_{j<i} B_{ij} \\ &\quad + (\rho_d r_d)^2 \frac{1}{2} \sum_{j \leq i} \sum_{k \leq i} C_{jk} f_j f_k \frac{m_j + m_k}{m_j m_k} X_{jk \rightarrow i} - (\rho_d r_d)^2 \sum_j C_{ij} f_i f_j \frac{1}{m_j} \end{aligned} \quad (11)$$

with:

$$S_{\alpha} = \sum_{i=1}^{M_{\alpha}} S_{\alpha,i} \Big|_{vel.group \alpha} \quad , \quad \sum_{\alpha=1}^N S_{\alpha} = 0 \quad (12)$$

where $B_{i,B}$ is the bubble birth rate due to breakup of larger bubbles, $D_{i,B}$ is the bubble death rate due to breakup of bubbles from size group i into smaller bubbles, $B_{i,C}$ is the bubble birth rate into size group i due to coalescence of smaller bubbles to bubbles belonging to size group i and finally $D_{i,C}$ is the bubble death rate due to coalescence of bubbles from size group i with other bubbles to even larger ones. B_{ij} and C_{ij} are the breakup and coalescence rates of bubbles from size groups i with bubbles of size group j . In eq. (11) m_i denotes the mass of the disperse phase allocated to bubble size group i and $X_{jk \rightarrow i}$ is the fraction of mass transferred to size group i due to coalescence of two bubbles from size groups j and k . Referring to the

original publications [9] and [10] these terms can be defined in dependence on gaseous phase velocity and size group properties and in dependence on fluid turbulence.

2.4 Remark on Cumulative Gaseous Phase Effects

It has to be mentioned, that for some physical modeling the splitting of the gaseous disperse phase into N velocity groups is rather artificial. E.g. the interfacial drag laws include a high void fraction correction exponent for the disperse phase volume fraction in order to account for dense particle effects in flow regions with comparable high gas volume fraction values. This correction of the bubble drag should be based on the total disperse phase volume fraction, rather than the volume group volume fraction. In the present model this cumulative gaseous phase effect has been taken into account. Since the drag coefficient is part of the FAD turbulent dispersion model in accordance with eq. (7), the high void fraction correction of the bubble drag affects the turbulent dispersion acting on individual velocity groups too – since bubble drag decreases for high void fraction the turbulent dispersion is locally decreased as well. Nevertheless turbulent dispersion of the bubble velocity groups in compliance with eq. (7) is still based on the gradient of the velocity group volume fraction. Similarly the bubble induced turbulence due to Sato's model is affected by the split of the total gas volume fraction on the N velocity groups, resulting in a slightly different predicted particle induced eddy viscosity. All these cumulative gaseous phase effects are subject to future investigations of the inhomogeneous MUSIG model.

3 VALIDATION AGAINST EXPERIMENTAL DATA

3.1 The TOPFLOW Test Facility at FZ Rossendorf

Experiments on the evolution of the radial gas fraction profiles, gas velocity profiles and bubble size distributions in a gas-liquid two-phase flow along a large vertical pipe of $D_I=194$ mm inner diameter have been performed at the TOPFLOW facility [15] in Rossendorf (Fig. 2). Two wire-mesh sensors were used to measure sequences of two-dimensional distributions of local instantaneous gas fraction within the complete pipe cross-section with a lateral resolution of 3 mm and a sampling frequency of 2500 Hz. This data is the basis for fast flow visualization and for the calculation of the mentioned profiles, which have been used for comparison with the CFD simulations and further validation of the inhomogeneous MUSIG model. The gas fraction profiles were obtained by averaging the sequences over time, velocities were measured by cross-correlation of the signals of the two sensors, which were located on a short (63 mm) distance behind each other. The high resolution of the mesh sensors allows identifying regions of connected measuring points in the data array, which are filled with the gas phase. This method was used to obtain the bubble size distributions.

In the experiments, the superficial velocities ranged from $J_G=0.04$ to 8 m/s for the gas phase and from $J_L=0.04$ to 1.6 m/s for the liquid, while we are focusing here on the experiment TOPFLOW-074 with $J_G=0.0368$ m/s and $J_L=1.017$ m/s for an air-water flow. In this way, the experiments cover the range from bubbly to churn turbulent flow regimes, where the selected test case belongs to the range of bubbly flow with breakup and coalescence and a developed core peak in the gas volume fraction profiles for the largest distance between gas injection and measurement cross-section. The evolution of the flow structure was studied by varying the distance between the gas injection and the sensor position. This distance was changed by the help of a so-called variable gas injection set-up (see Fig. 2). It consists of 6 gas injection units, each of them equipped with three rings of orifices in the pipe wall for the

gas injection. These rings are fed with the gas phase from ring chambers, which can be individually controlled by valves. The middle ring has orifices of 4 mm diameter, while the upper and the lower rings have nozzles of 1 mm diameter. In this way, 18 different inlet lengths and two different gas injection geometries can be chosen. The latter allows varying the initial bubble diameter at identical superficial velocities. For the test case 074 the 1mm orifices were used for gas injection. Therefore the development of the air-water flow can be studied from level R injection at $z=7.802\text{m}$ below the wire-mesh sensor up to level A injection at $z=0.221\text{m}$ below the measurement cross-section.

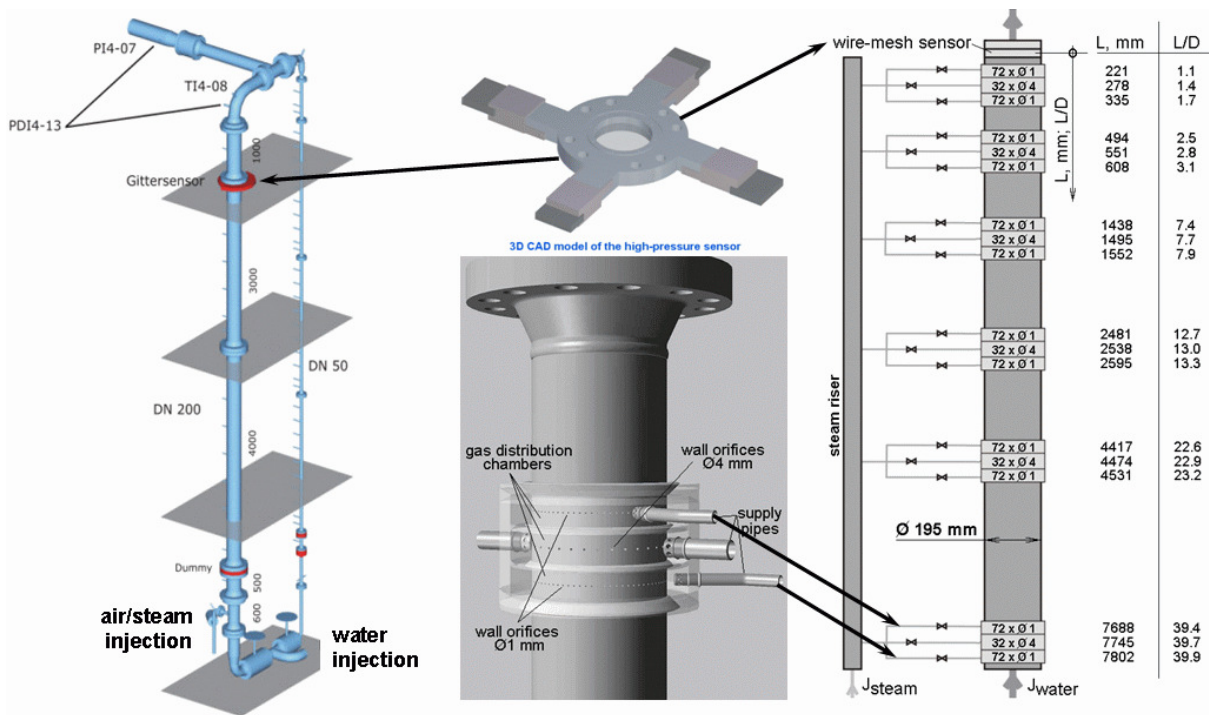


Figure 2: TOPFLOW test facility at FZ Rossendorf.

3.2 Application of a 3×7 Inhomogeneous MUSIG Model to the TOPFLOW-074 Test Case

For a first validation study of the inhomogeneous MUSIG model the test case TOPFLOW-074 has been selected, which is characterized by superficial air and water velocities of $J_G=0.0368\text{m/s}$ and $J_L=1.017\text{m/s}$, an isothermal temperature of 30°C and normal pressure. The pipe averaged gas volume fraction is still rather low for this test case at about $r_G\sim 3.5\%$. Nevertheless in large diameter pipes radial demixing of bubbles of different size or the present inlet BC's of gas injection can lead to locally high void fractions of more than 20% and breakup and coalescence processes gain in importance. For the vertical pipe flow geometry shown in Fig. 2, radial symmetry has been assumed, so that the numerical simulation was performed on a 60° radial sector of the pipe with symmetry boundary conditions (BC's) at both sides. At the outlet cross-section of the 10.0m long pipe section an averaged static pressure outlet BC has been applied. The pipe wall was assumed to be hydrodynamically smooth with a no-slip BC for water and a free-slip BC for the gaseous phase. The BC's for the SST turbulence model have been treated by the automatic wall function treatment of CFX-10 [17].

The inlet BC's for the liquid phase (water) at $z=-2.0\text{m}$ correspond to water velocity, turbulent kinetic energy and turbulent eddy frequency profiles of a fully developed single-phase pipe flow. The air void fraction at the inlet cross-section of the pipe has been set to zero. Gas is injected at $z=0.0\text{m}$ by point sources corresponding to the 12 individual 1mm wall orifices evenly distributed along the circumferential pipe wall of the 60° radial pipe sector. The injection velocity was calculated from the cross-section of the 1mm orifices and the gas mass flow defined by the given air superficial velocity.

For this first validation study of the inhomogeneous MUSIG model it was assumed, that the gaseous phase can be represented by 3 inhomogeneous velocity groups/phases with 7 bubble size classes in each group. Therefore an overall number of 21 bubble size classes have been used for the representation of the local bubble size distribution. The choice of 3 velocity groups was stimulated by the dependency of the Tomiyama lift force coefficient on the bubble diameter. This functional dependency shows for small bubbles a constant positive value of C_L , for large bubbles a constant negative value of C_L and an intermediate range of linear change of the lift force coefficient with increasing bubble diameter. Otherwise previous investigations had shown, that at least 15 bubble size groups are necessary for a certain accuracy of the breakup and coalescence models in the MUSIG model. The choice of 7 bubble size groups per velocity group is therefore a compromise between accuracy in the representation of the bubble size distribution and the resulting numerical effort for the solution of the large system of differential equations.

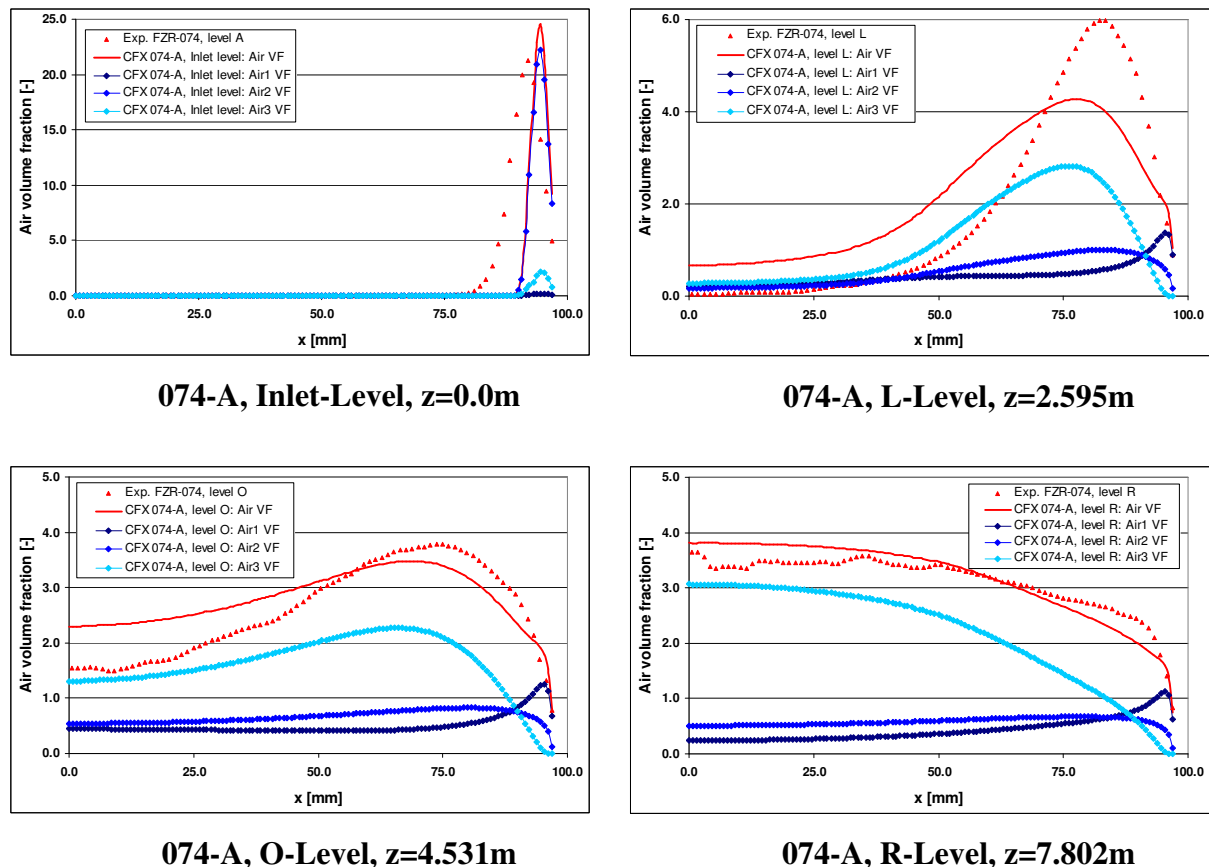


Figure 3: Comparison of TOPFLOW-074 gas volume fraction measurements with CFX-10 inhomogeneous 3x7 MUSIG model prediction 074-A at different pipe elevation levels.

The 21 bubble size classes were distributed according to an equal bubble diameter distribution with $\Delta d_p=0.619\text{mm}$ over the bubble size range of $d_p=0.01\text{mm}, \dots, 13\text{mm}$. The volume or size fraction distribution over these 21 bubble size classes for the wall orifice boundary conditions at $z=0.0\text{m}$ was derived from the level A gas volume fraction and bubble size measurements of TOPFLOW-074, i.e. for the smallest available distance between gas injection and measurement location in the experiments. The mean bubble diameter at gas injection location is about $d_p \sim 6.5\text{mm}$ and the narrow bubble size distribution is similar to a Gaussian profile.

The steady-state flow simulation was carried out on a hexahedral mesh generated with ICEM/CFD consisting of approx. 260.000 elements and 278.000 nodes. Geometric grid refinement had been applied to the near wall region and to the area of developing gas-liquid flow above the point of gas injection. The simulation had run on 8 AMD Opteron processors with a memory consumption of about 4.8 Gbyte and a simulation time of approx. 11 days.

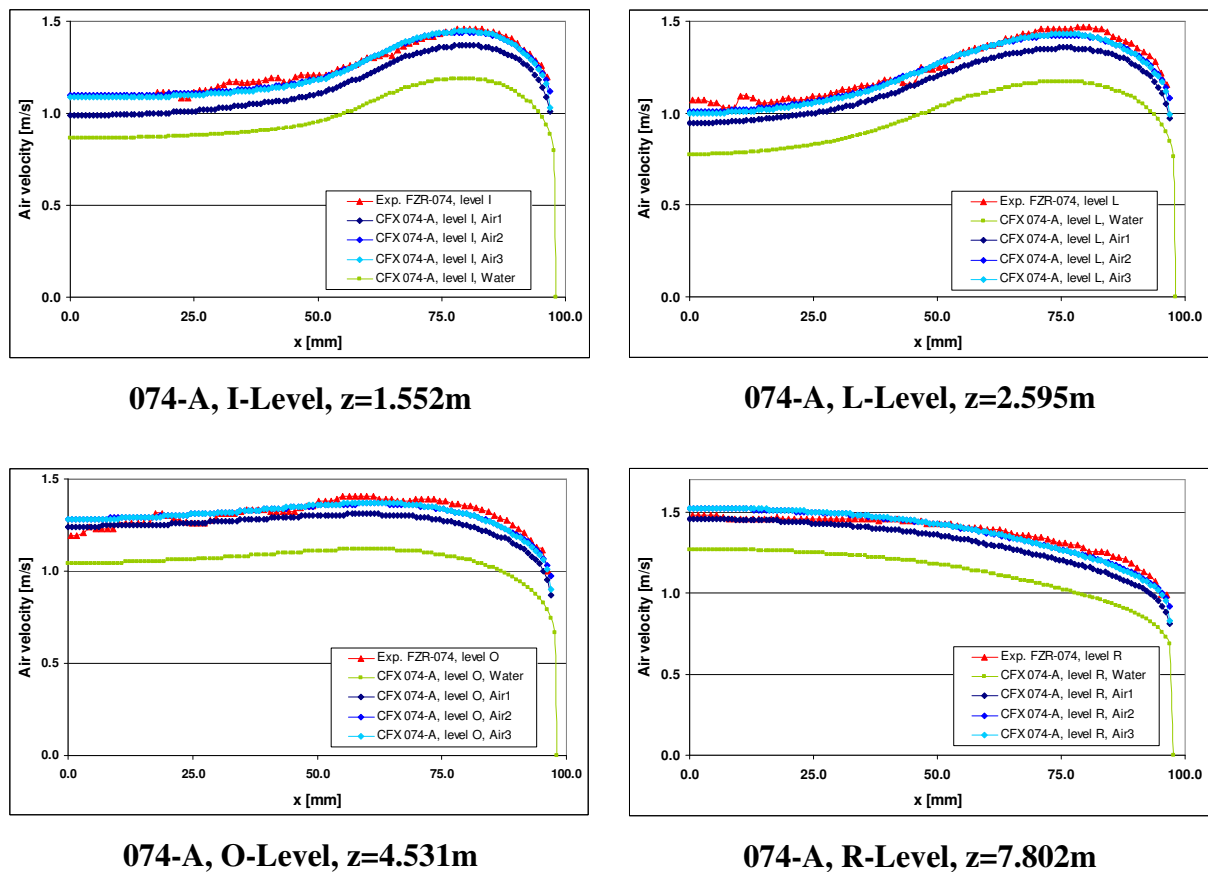


Figure 4: Measured and predicted (simulation 074-A) radial water and air velocity profiles for the TOPFLOW FZR-074 test case at the I-, L-, O- and R-level.

3.3 CFD Simulation vs. Experiment Comparison for TOPFLOW-074

Three different simulations have been carried out for the presented test case TOPFLOW-074 and have been compared with experimental data:

- **074-A:** bubble drag is calculated in correspondence with the Sauter mean diameter of a velocity group using Grace drag law [17]; a high void fraction correction exponent

of 4.0 was used, while the correction was based on the local void fraction of the velocity group; breakup model of Luo & Svendsen [9] and coalescence model of Prince & Blanch [10] were used without changes to the breakup and coalescence rates.

- **074-B:** bubble drag is calculated according to the Tomiyama drag correlation [18] using a high void fraction correction exponent of 4.0, while the correction is based on the local but cumulative air void fraction of the disperse phase; unchanged settings for the breakup and coalescence model parameters in comparison with 074-A.
- **074-C:** Since too high coalescence rates could be observed in simulations 074-A and 074-B, we reduced for this simulation the coalescence rates given by the Prince & Blanch model by a factor of 0.25 in order to study the model parameter influence on radial gas volume fraction distributions.

Results of the 074-A, 074-B and 074-C test case simulations are compared to gas volume fraction and gas velocity measurements at different elevations of the TOPFLOW test facility. In Fig. 3 and Fig. 6 each volume fraction profile of a velocity group (disperse phase) has been calculated as the cumulative sum of the volume fraction profiles of 7 corresponding bubble size classes. The cumulative air volume fraction profiles as compared in Fig. 5 represent the sum of gaseous phase void fraction over all 21 bubble size classes. Fig. 3 shows the axial development of the gas-liquid bubbly flow from the gas injection through wall orifices up to the uppermost measurement cross-section at R-level (simulation 074-A). At the injection level the gaseous phase is almost concentrated in a near wall bubble plume, where local gaseous phase volume fraction reaches as high levels as about 25%. Due to the prescribed inlet BC's gaseous phase belongs nearly entirely to the 2nd velocity group, while only a minor part of gas void fraction can be observed in the 3rd velocity group of large bubbles. Further diagrams in Fig. 3 show the axial development of the bubble plume arising from the wall orifices. At the same time, while the gas bubble plume is spreaded radially inwards by turbulent dispersion, coalescence of bubbles takes place leading to an increasing gas volume fraction in the bubble size classes with larger bubble diameters (in the velocity group Air3). Simultaneously large bubbles are decaying into smaller ones due to bubble breakup in boundary layer turbulence close to the wall. At the uppermost measurement cross-section at the R-level small bubbles (Air1) show a slightly pronounced wall peak, medium sized bubbles (Air2) are almost homogeneously distributed over the pipe cross section, while for the large bubbles (Air3) a remarkable core peak in the gas volume fraction profiles can be observed. The cumulative gas volume fraction profile finally shows a core peak, since most of the gaseous phase volume fraction had been reallocated to the velocity group of large bubbles due to coalescence. Also it can be observed that the gas bubble plume injected through the wall orifices is spreading a little bit too fast, the established accuracy and agreement with the experimental data for the axial development of gas volume fraction profiles is remarkably good with respect to the complexity of the flow.

Fig. 4 shows the comparison of radial velocity profiles of the liquid phase and velocity groups with measured gas velocities (074-A). The agreement is very good at all pipe elevation levels. Especially for the lower I- and L-levels a near wall deformation of the radial water velocity profile due to the wall orifice gas injection and the buoyancy of the developing gas bubble plume can be observed. In fully developed state at R-level the water velocity profile is then again comparable to fully developed turbulent pipe flow profile. The smaller slip velocity of the small bubbles velocity group is caused by the higher drag of small bubbles.

If we look on the distribution of the cumulative gas volume fraction over the three velocity groups, then it could be observed from 074-A simulation results (Fig. 3), that a too high void fraction was finally found in the large bubbles velocity group (Air3) due to a too strong coalescence. Furthermore it was observed, that the initial near wall bubble plume was

spreaded too fast in terms of radial propagation and lowering of the maximum void fraction. This both observations gave rise to further investigations of 074-B and 074-C simulations.

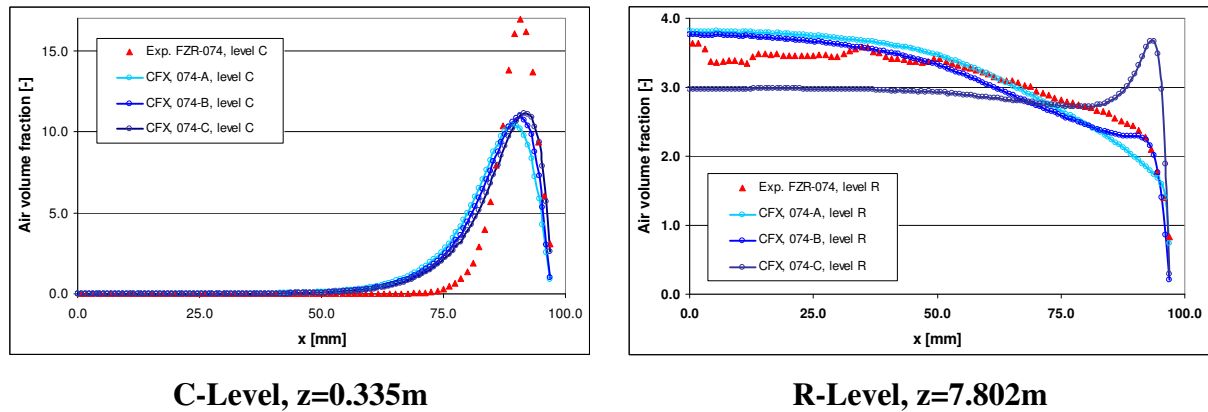


Figure 5: Comparison of cumulative radial air volume fraction profiles for TOPFLOW-074 test case simulations 074-A, -B and -C at the C- and R-level.

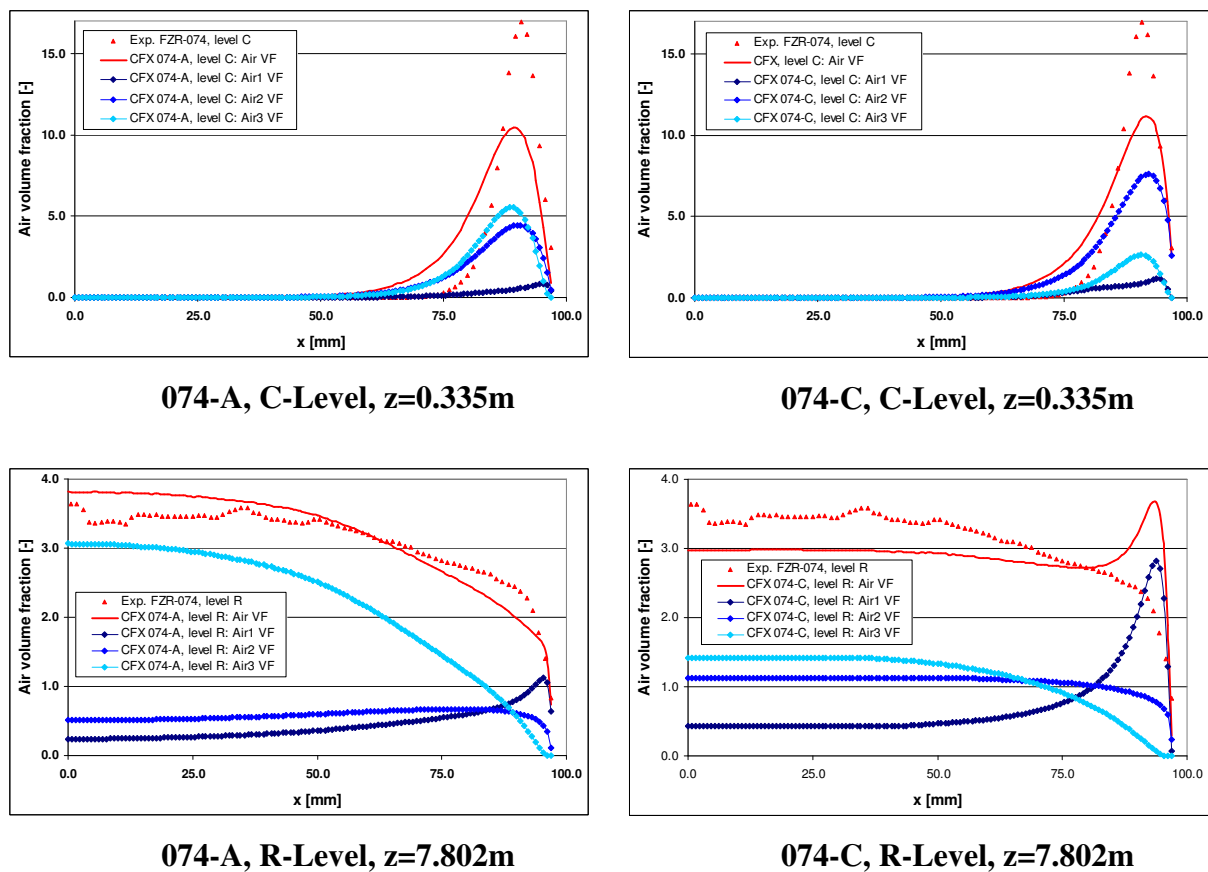


Figure 6: Comparison of homogeneous volume group resolved radial volume fraction profiles for TOPFLOW-074 test case simulation 074-A and 074-C at C- and R- levels.

Fig. 5 shows the direct comparison of the cumulative gaseous phase volume fraction profiles for these three simulation runs. It can be observed from the C-level diagram, that the changes in high void fraction bubble drag coefficient correction and related turbulent dispersion force changes had almost no effect on the cumulative void fraction distribution at lower pipe elevations. Otherwise the reduced coalescence rates in 074-C lead to a higher amount of gas volume fraction in the small bubble velocity group (Air1) due to relatively more pronounced breakup processes. Since small bubbles are shifted by lift force towards the pipe wall we can observe a near wall maximum in the gas volume fraction profile at the R-level.

Fig. 6 highlights the effect of reduced coalescence rates in 074-C in more detail by comparing the velocity group resolved volume fraction profiles with 074-A simulation results. While in 074-A the void fraction accumulated in Air2 and Air3 is almost equal at C-level, the same gas volume fraction profile is still dominated by the Air2 volume fraction distribution for 074-C simulation. High coalescence rates in 074-A lead to a shift of about 75% of overall gas volume fraction to the large bubble velocity group (Air3). In contrary for 074-C gas volume fraction is almost evenly distributed amongst the three velocity groups, but unfortunately leading to a non-physical near wall void fraction maximum and lowered void fraction level in the pipe core. Best agreement with experimental data was therefore established for the 074-B simulation conditions and more detailed investigations of the turbulent dispersion, breakup and coalescence models are necessary in order to resolve the remaining differences.

CONCLUSION

The paper presents model derivation and validation of a new population balance method for the prediction of polydispersed bubbly flows. The so-called inhomogeneous Multiple Size Group (MUSIG) model is based on the multi-fluid Eulerian approach, where the gaseous phase is divided by bubble diameter into a number N of velocity groups or phases, where each of them has its own velocity field information. In order to apply population balance methods for the consideration of bubble breakup and coalescence processes each of the velocity groups can be divided into a larger number of bubble size groups. Bubble size dependent drag, lift and turbulent dispersion forces are taken into account in the momentum transport equations solved for each velocity group. Thereby the inhomogeneous MUSIG model facilitates the prediction of radial demixing of bubbles of different sizes as it is observed in polydisperse bubbly flows.

Furthermore validation of the inhomogeneous MUSIG model has been carried out for test case conditions of the TOPFLOW-074 experiment at FZR. Good agreement was found for the comparison of predicted radial bubble size resolved volume fraction and velocity profiles against experimental data at different measurement cross-sections of the TOPFLOW facility. The remaining issues of a too fast spread of the bubble plume arising from gas injection orifices and observed differences in the finally predicted bubble size spectrum need further detailed investigation of the bubble breakup and coalescence models as well as the usage of a larger database of detailed and reliable experimental data at different flow conditions.

ACKNOWLEDGMENTS

This research has been supported by the German Ministry of Economy and Labour (BMWA) in the framework of the German CFD Network on Nuclear Reactor Safety Research and Alliance for Competence in Nuclear Technology, Germany.

REFERENCES

- [1] A. Tomiyama: "Struggle with computational bubble dynamics", *ICMF'98, 3rd Int. Conf. Multiphase Flow*, Lyon, France, pp. 1-18, June 8.-12. 1998.
- [2] M. Sommerfeld, E. Bourloutski, D. Bröder: "Euler/Lagrange calculations of bubbly flows with consideration of bubble coalescence", *CJChE - The Canadian journal of chemical engineering*, Vol. 81, pp. 508-518, 2003.
- [3] M. Sommerfeld: "Detailed Modelling of Elementary Processes in Bubbly Flows on the Basis of the Lagrangian Approach", 3rd Joint ANSYS & FZR Workshop on Multiphase Flows, Rossendorf, Germany, 31. May-3. June 2005.
- [4] B. Bunner, G. Tryggvason, "Simulations of Large Bubble Systems" ASME Fluids Engineering Division Summer Meeting, Vancouver, Canada, June 22-26, 1997.
- [5] B. Bunner, G. Tryggvason, "Direct Numerical Simulations of Three-Dimensional Bubbly Flows", *Phys. Fluids*, Vol. 11 (1999), pp. 1967-1969.
- [6] M.F. Göz, B. Bunner, M. Sommerfeld, G. Tryggvason: "Microstructure of a bidisperse swarm of spherical bubbles", Joint US ASME/European Fluids Engineering Summer Conference, Montreal, Paper No. FEDSM 2002-31395 (2002).
- [7] M. Wörner, B. Ghidersa, A. Onea: "Direct Numerical Simulation of Bubble Train Flow in a Square Mini-Channel and Evaluation of Liquid Phase Residence Time Distribution", 3rd Joint ANSYS & FZR Workshop on Multiphase Flows, Rossendorf, Germany, 31. May-3. June 2005.
- [8] S. Lo: "Modeling of bubble breakup and coalescence with the MUSIG model", AEA Technical Report No. AEAT-4355, Issue 1, pp. 1-12, October 1998.
- [9] H. Luo, H.F. Svendsen: "Theoretical model for drop and bubble breakup in turbulent dispersion", *AIChE J.*, Vol. 42, No. 5, pp. 1225-1233, 1996.
- [10] M.J. Prince, H.W. Blanch: "Bubble coalescence and break-up in air-sparged bubble columns", *AIChE J.*, Vol. 36, No. 10, pp. 1485-1499, 1990.
- [11] A. Tomiyama, N. Shimada: "(N+2)-field modeling for bubbly flow simulation", *Computational Fluid Dynamics Journal*, Vol. 9, No. 4, pp. 418-426 (2001).
- [12] J. Shi, Th. Frank, H.-M. Prasser, U. Rohde: "Nx1 MUSIG model – Implementation and application to gas-liquid flows in vertical pipe", 22. CADFEM & ANSYS CFX Users Meeting, Dresden, Germany, 9.-12. November 2004.
- [13] Th. Frank: "Advances in Computational Fluid Dynamics (CFD) of 3-dimensional gas-liquid multiphase flows", NAFEMS Seminar "Simulation of Complex Flows (CFD)", Wiesbaden, Germany, April 25-26, 2005, pp. 1-18.
- [14] J.-M. Shi, P.J. Zwart, Th. Frank, U. Rohde, H.-M. Prasser: "Development of a multiple velocity multiple size group model for poly-dispersed multiphase flows", p.21-26, Annual Report 2004, Forschungszentrum Rossendorf, Germany, 2004.

- [15] H.-M. Prasser, D. Lucas, E. Krepper, D. Baldauf, A. Böttger, U. Rohde et al.: „Strömungskarten und Modelle für transiente Zweiphasenströmungen“, Forschungszentrum Rossendorf, Germany, Report No. FZR-379, pp. 183, June 2003.
- [16] H.-M. Prasser, M. Beyer, H. Carl, S. Gregor, D. Lucas, P. Schütz, F.-P. Weiss: “Evolution of the Structure of a Gas-Liquid Two-Phase Flow in a Large Vertical Pipe”, The 11th International Topical Meeting on Nuclear Reactor Thermal-Hydraulics (NURETH-11), Popes Palace Conference Center, Avignon, France, October 2-6, 2005.
- [17] CFX-10 User Manual, ANSYS-CFX, July 2005.
- [18] T. Takamasa, A. Tomiyama: “Three-dimensional gas-liquid two-phase bubbly flow in a C-shaped tube”, 9th Int. Topical Meeting on Nucl. React. Thermal Hydraulics (NURETH-9), San Francisco, California, October 3-8, 1999, pp. 1-17.
- [19] Th. Frank, J.-M. Shi, A.D. Burns: “Validation of Eulerian multiphase flow models for nuclear reactor safety applications”, 3rd International Symposium on Two-phase Flow Modeling and Instrumentation, Pisa, 22.-24. Sept. 2004, pp. 1-9.